Dual-Band Wireless Power Transmitter with Reconfigurable Power Amplifier and "Decoupling Ring"

Yaoxia Shao[1],Ming Liu[2],Huan Zhang[1],Chengbin Ma[1],
[1]*University of Michigan-Shanghai Jiao Tong University Joint Institute,*
Shanghai Jiao Tong University, Shanghai, P. R. China
[2]*Dept. of Electrical Engineering, Princeton University, Princeton, NJ, USA*
yaoxiashao@sjtu.edu.cn, chbma@sjtu.edu.cn, ml45@princeton.edu

***Abstract*—There are 2 wireless power standards for the mobile device market: Qi standard and AirFuel standard with frequencies of hundreds of kHz and 6.78 MHz. This paper presents a dual-band wireless transmitter operating at both 200 kHz and 6.78 MHz. A dual-band reconfigurable PA with Class E and half-bridge modes is introduced to decrease the size of transmitter. Meanwhile, the eddy current loss model of parallel connected dual-band coils is established to provide guidance for coil design. Finally, a dual-band charging pad with specially designed "decoupling ring" is proposed, which can effectively reduce the extra loss of dual-band operation.**

***Index Terms*—Multi mode, dual band, multistandard, wireless power transfer, inductive power transfer, MHz.**

I. Introduction

In the past few years, consumer electronic products such as mobile phones and wearable devices equipped with wireless charging have become pervasive [1]. To ensure compatibility among different products, industry leaders have established wireless power transfer (WPT) standards [2], such as Qi and AirFuel with operating frequencies from hundreds of kHz to several MHz. However, it is not a satisfying situation to have multiple standards that are incompatible since it cause inconvenience to consumers [3].

Qi standard operating at 87$\sim$205 kHz is proposed by the Wireless Power Consortium (WPC), which applies relatively tight coupling between Tx and Rx coils. Qi has the advantages of high efficiency, good compatibility and in-band communication. To obtain smaller size and larger charging spatial freedom, a new operating frequency of 6.78 MHz for WPT have received more and more attention [4]. Therefore, AirFuel operating at 6.78 MHz becomes another competitive candidate WPT standard.

There has been a lot of related research on the circuit topology, coils and control of kHz WPT. However, realizing MHz WPT system with high efficiency and robustness is more challenging due to increased gate power dissipation and cost. Researchers have made efforts to investigate PA [5]–[7] and rectifier which are more suitable for MHz WPT. Among these researches, Class E typology (PA, rectifier) shows its superiority at MHz operation due to low switching loss and total harmonic distortion (THD) [8].

For the above discussions, there is a need to develop multistandard solutions which are compatible with both kHz and MHz WPT. [9] proposed a dual-band receiver which can operates at 100 kHz and 6.78 MHz. But in fact, Rx side often has more strict size constraints than Tx side [10]. Therefore, it is more realistic to design transmitters with dual-band capability.

The main challenges of designing a dual-band wireless power transmitter are: 1) The transmitter volume should be limited, therefore embedded coil layout is preferred; 2) Circuit complexity and number of components should be minimized, by using reconfigurable PA with switchable modes; 3) The extra eddy current loss brought by dual-band operation should be minimized; 4) The effect of kHz ferrite on megahertz charging should be reduced.

This paper proposed a dual-band wireless power transmitter for 200 kHz and 6.78 MHz with a few novel topologies and architectures: In order to reduce the cost of components, a dual-band reconfigurable PA with Class E and half-bridge mode is proposed. Besides, a dual-band charging pad is designed with the "decoupling ring", based on detailed analysis on eddy current loss of the coils.

II. Proposed Dual-Band Wireless Power Transmitter

The system configuration of the WPT system with proposed dual-band transmitter is illustrated in Fig. 1 (a). It consists of a dual-band reconfigurable power amplifier (DBRPA), a high-frequency (HF) coil, a low-frequency (LF) coil as well as their corresponding receivers. The transmitter can charge one Qi receiver at kHz or multiple AirFuel receivers at MHz. If both LF and HF receivers need to be charged at the same time, the transmitter may adopt the time-sharing strategy since the DBRPA cannot provide kHz and MHz power concurrently. Note that both receivers of HF and LF are represented by R_{HFrec} and R_{LFrec} for simplicity.

A. Dual-Band Reconfigurable Power Amplifier (DBRPA)

There are several ways to generate MHz and kHz power in a single transmitter. A common way is to equip both the HF

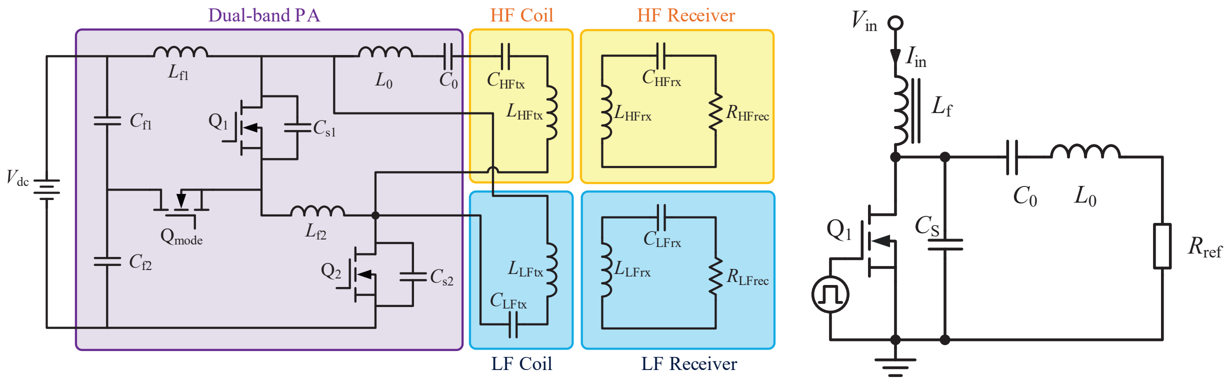

(a) (b)

Fig. 1. (a) Schematic of the dual-band WPT system. (b) The configuration of single-end Class E PA.

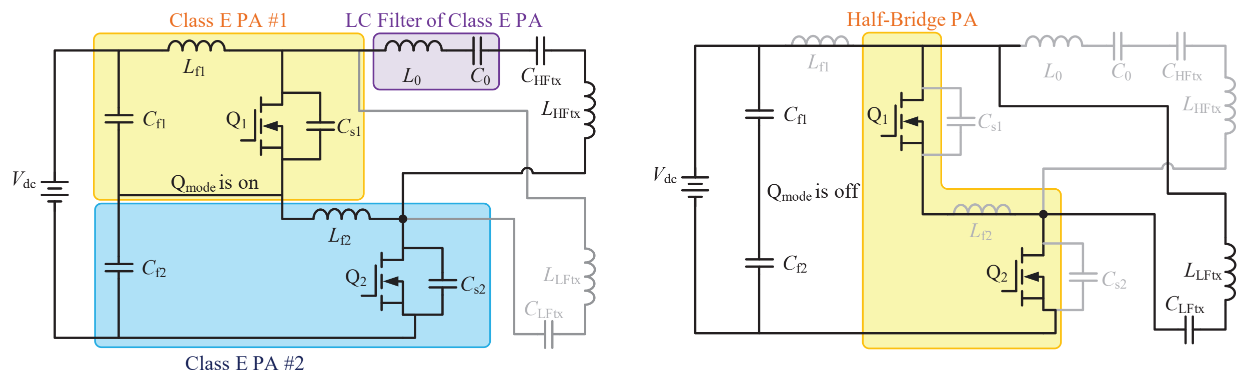

(a) (b)

Fig. 2. Typology of the dual-band reconfigurable PA (a) Operating at HF with Q_{mode} ON. (b) Operating at LF with Q_{mode} OFF.

PA (e.g. Class E, Class EF) and LF PA (e.g. full-bridge, half-bridge). The advantage of this approach is that the HF and LF coils can operate concurrently [10]. However, additional components, especially switching devices such as MOSFETs will increase the cost and size of the transmitter. Another strategy is to design a reconfigurable PA which can switch between HF and LF modes, such as the modified multi-mode ZVS Class D PA presented in [3].

Compared with traditional bridge PAs, Class E PA owns the advantage of ZVS and ZVDS operation, i.e., both the voltage and voltage derivative of the MOSFET attain zero when switching on, dramatically decreasing the switching loss when operating at several MHz. A typical single-end Class E PA is shown in Fig. 1 (b).

This paper proposed a DBRPA with Class E and half-bridge modes, based on the dual-band rectifier typology presented in [11]. As shown in Fig. 1 (a), the PA consists of a low-speed mode selection switch Q_{mode}, two shunt capacitors C_{s1} and C_{s2}, two RF choke inductors L_{f1} and L_{f2} as well as two switches Q_1 and Q_2. Fig. 2 (a) and Fig. 2 (b) show the operation principle of the proposed PA. If Q_{mode} is turned on, the PA functions as a push-pull Class E PA with two single-end Class E PAs connected in series, generating HF (e.g. 6.78 MHz) power. Meanwhile L_0 and C_0 form the LC filter network of the push-pull Class E PA. If Q_{mode} is kept off, the PA acts as a half-bridge Class D PA, since the RF chokes can be regarded as short and the shunt capacitors can be regarded as open when operating at LF (e.g. 200 kHz). Note that time-sharing strategy is applied when both LF and HF receivers need to be charged, i.e., the PA switches between LF and HF modes regularly to ensure all the receivers placed on the charging pad can be charged.

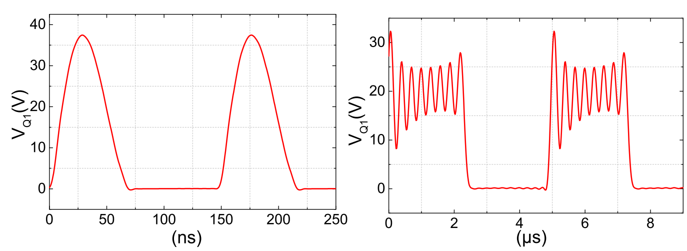

(a) (b)

Fig. 3. (a) Simulated drain-to-source voltage of Q_{s1} at 6.78 MHz. (b) Simulated drain-to-source voltage of Q_{s1} at 200 kHz.

The simulated voltage waveforms of the switches working at HF (6.78 MHz) and LF (200 kHz) are shown in Fig. 3. At HF mode, the PA realize ZVS and ZVDS soft-switching. At LF mode, the PA generates square-wave voltage, which includes a HF ripple due to the oscillation caused by L_f and C_s. This is a compromise that comes with merging the two typologies.

B. Eddy Current Loss at 6.78 MHz Operation Mode

A major challenge for dual-band transmitter is to prevent the eddy current loss in LF coil when the system operates at HF mode. One common way is to add a LC parallel network of which the resonant frequency is 6.78 MHz to the LF path. However, the LF operating efficiency is decreased due to the network [10]. Meanwhile, additional components increase the cost and size. In order to investigate other methods to restrict eddy current loss, it is necessary to analytically derive the dual-band loss model.

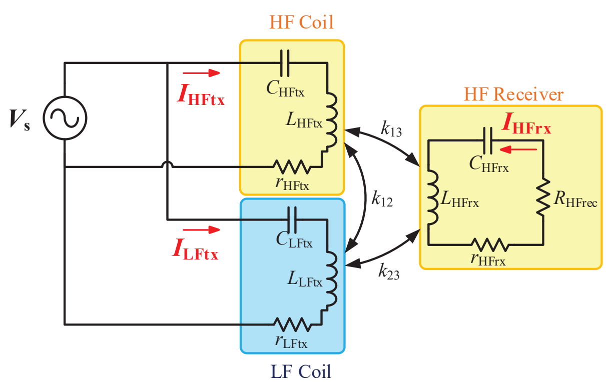

Fig. 4. Circuit model for coil analysis at 6.78 MHz

The circuit model of HF power transfer is illustrated in Fig. 4. Here r with different subscripts denotes the parasitic resistances of coils, and k with different subscripts denotes the coupling coefficients between coils. V_s is the 6.78 MHz voltage source. The model can be characterized by Kirchoff's voltage law as:

$$
\begin{aligned}
\boldsymbol{V_s} &= \left(r_{HFtx} - \frac{j}{\omega C_{HFtx}} + j\omega L_{HFtx}\right)\boldsymbol{I_{HFtx}} \\
&\quad + j\omega k_{13}\sqrt{L_{HFrx}L_{HFtx}}\boldsymbol{I_{HFrx}} \\
&\quad + j\omega k_{12}\sqrt{L_{HFtx}L_{LFtx}}\boldsymbol{I_{LFtx}}, \\
\boldsymbol{V_s} &= \left(r_{LFtx} - \frac{j}{\omega C_{LFtx}} + j\omega L_{LFtx}\right)\boldsymbol{I_{LFtx}} \\
&\quad + j\omega k_{13}\sqrt{L_{HFrx}L_{HFtx}}\boldsymbol{I_{HFrx}} \\
&\quad + j\omega k_{12}\sqrt{L_{HFtx}L_{LFtx}}\boldsymbol{I_{LFtx}}, \\
0 &= \left(r_{HFrx} - \frac{j}{\omega C_{HFrx}} + j\omega L_{HFrx} + R_{HFrec}\right)\boldsymbol{I_{HFrx}} \\
&\quad + j\omega k_{13}\sqrt{L_{HFrx}L_{HFtx}}\boldsymbol{I_{HFtx}} \\
&\quad + j\omega k_{23}\sqrt{L_{HFrx}L_{LFtx}}\boldsymbol{I_{LFtx}},
\end{aligned} \tag{1}
$$

where ω is the 6.78 MHz operating frequency, $\boldsymbol{I_{HFtx}}$, $\boldsymbol{I_{LFtx}}$ and $\boldsymbol{I_{HFrx}}$ are current phasors. Here Mathematica is used to solve for the currents. The complex analytical expressions of the current phasors are not shown here, which are illustrated graphically in the following. Note that the coils and capacitors satisfy the condition for resonance:

$$
\begin{aligned}
C_{HFtx} &= \frac{1}{\omega^2 L_{HFtx}}, \\
C_{HFrx} &= \frac{1}{\omega^2 L_{HFrx}}, \\
C_{LFtx} &= \frac{1}{\omega_{LF}^2 L_{LFtx}},
\end{aligned} \tag{2}
$$

where ω_{LF} is the 200 kHz operating frequency. The normalized eddy current can be formulated as:

$$
I_{eddy,norm} = \frac{I_{eddy}}{I_o} = \frac{|\boldsymbol{I_{LFtx}}|}{|\boldsymbol{I_{HFrx}}|}, \tag{3}
$$

where $|\boldsymbol{I_{LFtx}}|$ and $|\boldsymbol{I_{HFrx}}|$ are the amplitudes of eddy current in the LF Tx coil and output current in the HF Rx coil, separately. Higher $I_{eddy,norm}$ means higher eddy current occurs when the same current is generated in the Rx coil. To graphically analyze the influence of different parameters on eddy current, we set default system parameters as shown in Table I.

Intuitively, the coupling coefficient between the two Tx coils has greatest impact on the eddy current, which is verified in Fig. 5 (a). To accurately quantify the loss due to eddy current, the normalized eddy current loss is defined as:

$$
P_{eddy,norm} = \frac{P_{eddy}}{P_{in}} = \frac{|\boldsymbol{I_{LFtx}}|^2 r_{LFtx}}{\mathrm{Re}\left[\boldsymbol{V_s}\cdot(\boldsymbol{I_{HFtx}}+\boldsymbol{I_{LFtx}})^*\right]}, \tag{4}
$$

and normalized total loss is also defined as:

$$
\begin{aligned}
P_{loss,norm} &= \frac{P_{loss}}{P_{in}} = \frac{P_{in}-P_o}{P_{in}} = 1-\eta \\
&= 1 - \frac{|\boldsymbol{I_{HFrx}}|^2 R_{HFrec}}{\mathrm{Re}\left[\boldsymbol{V_s}\cdot(\boldsymbol{I_{HFtx}}+\boldsymbol{I_{LFtx}})^*\right]},
\end{aligned} \tag{5}
$$

where R_{HFrec} is the input resistance of the rectifier. By plotting (4) and (5) with the default parameters, as shown in Fig. 5 (b), we find that as k_{12} increases, eddy current becomes the main cause of the total power loss. This implies that it is effective to reduce the eddy current loss by reducing the cross coupling between LF and HF Tx coils.

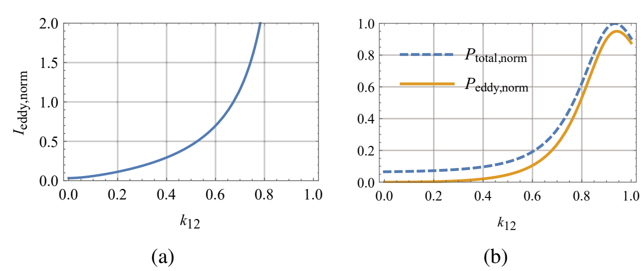

Fig. 5. (a) Normalized eddy current in the LF Tx coil when the transmitter operates at 6.78 MHz. (b) Normalized eddy current loss in the LF Tx coil and normalized total power loss of the WPT system when the transmitter operates at 6.78 MHz.

TABLE I
DEFAULT SYSTEM PARAMETERS OF THE DUAL-BAND WPT SYSTEM

L_{HFtx} (μH)	r_{HFtx} (Ω)	L_{LFtx} (μH)	r_{LFtx} (Ω)	L_{HFrx} (μH)	r_{HFrx} (Ω)	k_{13}	k_{23}	R_{HFrec} (Ω)
3	0.5	5	1.5	0.8	0.2	0.15	0.05	5

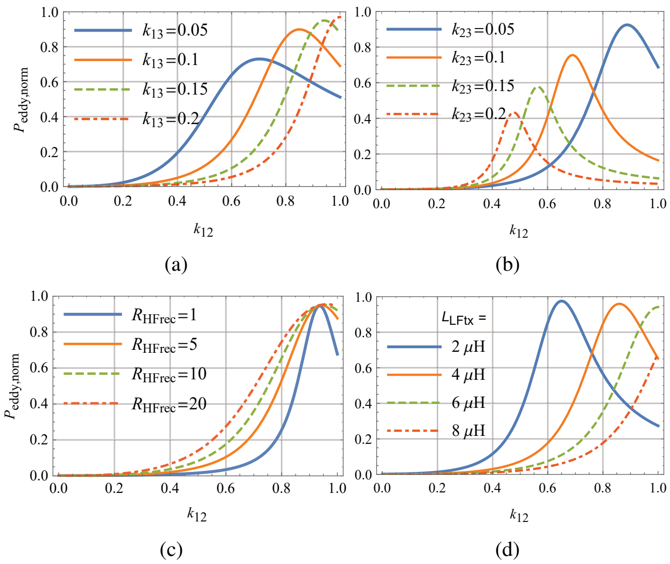

Fig. 6. Normalized eddy current loss in the LF Tx coil when tuning different system parameters.(a) Tuning the coupling coefficient k_{13} between HF Tx and HF Rx coils. (b) Tuning the coupling coefficient k_{23} between LF Tx and HF Rx coils. (c) Tuning the load R_{HFrec}. (b) Tuning the inductance L_{LFtx} of LF Tx coil.

By using the "Manipulate" function in Mathematica, the system parameters that have significant impact on the normalized eddy current loss can be found easily, with the tuning results shown in Fig. 6. From the figure, the key parameters and corresponding methods for reducing eddy current loss can be concluded as:

- The coupling coefficient k_{12} between HF and LF coils has the greatest effect on eddy current loss. Therefore, innovative design of Tx coils, which reduces k_{12} without the increase in transmitter size, is a good choice;
- Larger k_{13} and smaller k_{23} are helpful to lower eddy current loss. This implies that distinct HF and LF charging areas should be set on the charging pad. Therefore when HF receiver is put on the HF zone, relatively large k_{13} and small k_{23} can be obtained;
- A smaller load R_{HFrec} helps to decrease eddy current loss. Thus, increasing the charging current in the HF receiver is an effective solution, since $I_{HFrx} = \sqrt{P_o/R_{HFrec}}$;
- LF Tx coil with higher inductance is preferred to prevent the penetration of eddy current.

It should be noted that there are some other parameters that also can influence the eddy current. But they may have double effects, e.g., the eddy current may be reduced by lowering the inductance L_{HFtx}, but other loss can be increased through such adjustment.

C. Dual-Band Charging Pad with "Decoupling Ring"

In order to effectively utilize the area of charging pad and to take advantage of high spatial freedom of MHz WPT, it is reasonable to design the dual band charging pad with outer MHz coil and inner kHz coil. However this layout with high cross coupling makes additional filter essential to restrict the eddy current loss. Moreover, the ferrite under LF coil may affect the operation of HF mode. As discussed in the previous subsection, it is preferred to design a dual-band charging pad with distinct HF and LF areas and low cross coupling between HF and LF Tx coils. In the following, a novel charging pad with a decoupling ring is introduced.

First, by applying Biot-Savart's law, we derive z component of the magnetic field at (x, y, z) of a single-turn coil as:

$$B_z = \int_0^{2\pi} \frac{IR\mu_0 \left[R - x\cos\theta - y\sin\theta\right]}{4\pi \left[z^2 + (x - R\cos\theta)^2 + (y - R\sin\theta)^2\right]^{3/2}} \mathrm{d}\theta, \tag{6}$$

where $\mu_0 = 4\pi \times 10^{-7}\ H/m$ is the permeability of free space, I is the current amplitude and R is the radius of the coil. Fig. 7 shows B_z of the single-turn coil at $z = 0$.

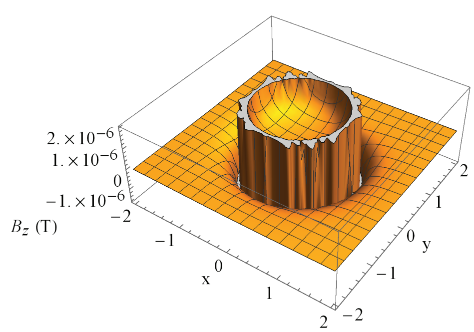

Fig. 7. z component of the magnetic field of a single-turn coil in $z = 0$ plane

If the HF Tx coil is designed as a series connection of two concentric coils with different radii and opposite directions, it may produce a zero-magnetic-field region near the center of the coils, where the LF coil is placed. This can decouple two Tx coils theoretically. The inner HF coil which cancel the magnetic field inside is called the "decoupling ring".

Here, we design a tool based on (6) to choose the parameters of such a HF coil with the decoupling ring. As shown in Fig. 8, one may adjust the radii and number of turns ("$-$" sign indicates the currents in the inner and outer coils flow at the opposite direction) of the outer and inner coils. With parameters shown in the figure ($R_{outer} = 75\ mm,\ R_{inner} = 28\ mm,\ N_{outer} = 3,\ N_{inner} = -1$), we can design a HF

Tx coil with the decoupling ring. The overall layout of the charging pad is illustrated in Fig. 9, which includes the MHz coil with outer coil and inner decoupling ring, the kHz coil as well as its ferrite. Note that since the HF coil generates no magnetic field inside the decoupling ring, the ferrite of LF coil does not impact the HF charging mode theoretically, which is another advantage of such design.

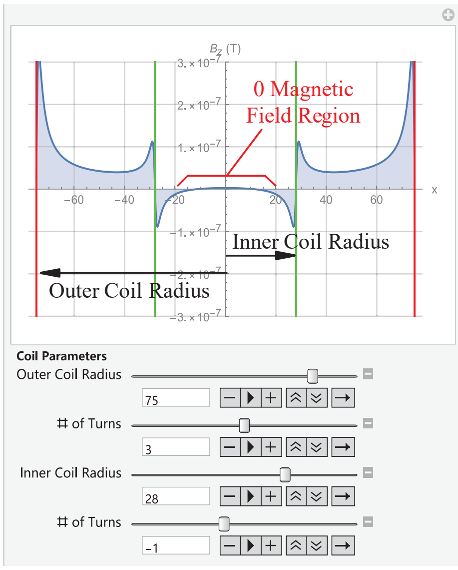

Fig. 8. Design tool panel for designing HF coil with decoupling ring.

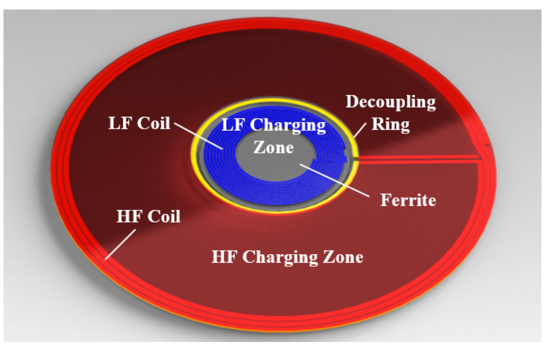

Fig. 9. Dual-band wireless charging pad structure.

To validate the proposed dual-band charging pad, High Frequency Structure Simulator (HFSS) is used to perform finite element simulations. Fig. 10 compares the magnetic field intensity of the coils designed with and without the decoupling ring, individually. The simulation results are in good agreement with the theoretical analysis. The proposed HF coil not only produces a weak-magnetic-field region inside the inner ring, but also enhances the magnetic field in the HF charging region, thereby increasing the coupling coefficient between HF Tx and Rx coils.

Other parameters of the coupling coils are also simulated, with the simulation layout shown in Fig. 11. And the simulation results are listed in Table II. It can be seen that the cross coupling between the two Tx coils is very small ($k_{12} = 0.0065$), and the coupling coefficient between HF Tx and Rx coils is large enough (($k_{13} = 0.15$)) to efficiently transmit MHz power.

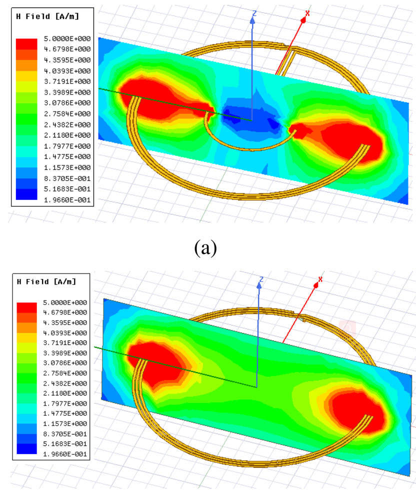

(a)

(b)

Fig. 10. Simulated magnetic field of HF Tx coils. (a) Tx coil with the decoupling ring. (b) Normal Tx coil without the decoupling ring.

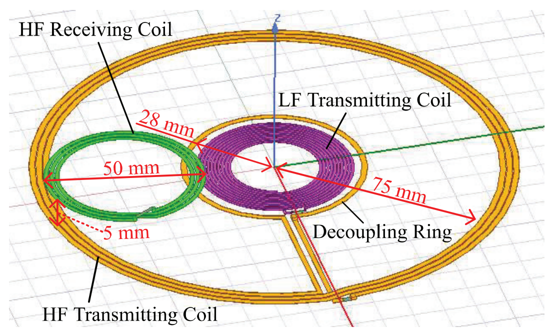

Fig. 11. Layout of coupling coefficient and inductance simulation.

III. Conclusions

kHz operation offers higher efficiency and power rating while MHz operation offers higher spatial freedom and smaller size [11]. A well-designed dual band transmitter should possess both advantages of LF and HF WPT with reasonable and effective control of extra power loss and cost. This paper takes common pain points of traditional dual-band wireless power transmitters into consideration, proposes a more integrated dual-band transmitter with the reconfigurable PA and decoupling ring. Subsequent research will focus on prototype design and experimental verification.

References

[1] M. Fu, Z. Tang, and C. Ma, "Analysis and optimized design of compensation capacitors for a megahertz wpt system using full-bridge rectifier," *IEEE Transactions on Industrial Informatics*, vol. 15, no. 1, pp. 95–104, 2018.

[2] D. Van Wageningen and T. Staring, "The qi wireless power standard," in *Proceedings of 14th International Power Electronics and Motion Control Conference EPE-PEMC 2010*. IEEE, 2010, pp. S15–25.

TABLE II
SIMULATED SYSTEM PARAMETERS OF THE DUAL-BAND WPT SYSTEM

L_{HFtx} (μH)	r_{HFtx} (Ω)	L_{LFtx} (μH)	r_{LFtx} (Ω)	L_{HFrx} (μH)	r_{HFrx} (Ω)	k_{12}	k_{13}	k_{23}
3.27	0.61	5.16	1.33	0.76	0.18	0.0065	0.15	0.039

[3] M. de Rooij and Y. Zhang, "A 10 w multi-mode capable wireless power amplifier for mobile devices," in *PCIM Asia 2016; International Exhibition and Conference for Power Electronics, Intelligent Motion, Renewable Energy and Energy Management*. VDE, 2016, pp. 1–8.

[4] S. Liu, M. Liu, S. Yang, C. Ma, and X. Zhu, "A novel design methodology for high-efficiency current-mode and voltage-mode class-e power amplifiers in wireless power transfer systems," *IEEE Transactions on Power Electronics*, vol. 32, no. 6, pp. 4514–4523, 2016.

[5] S. Aldhaher, P. C.-K. Luk, A. Bati, and J. F. Whidborne, "Wireless power transfer using class e inverter with saturable dc-feed inductor," *IEEE Transactions on Industry Applications*, vol. 50, no. 4, pp. 2710–2718, 2014.

[6] M. Liu, M. Fu, and C. Ma, "Low-harmonic-contents and high-efficiency class e full-wave current-driven rectifier for megahertz wireless power transfer systems," *IEEE Transactions on Power Electronics*, vol. 32, no. 2, pp. 1198–1209, 2016.

[7] P. Srimuang, N. Puangngernmak, and S. Chalermwisutkul, "13.56 mhz class e power amplifier with 94.6% efficiency and 31 watts output power for rf heating applications," in *2014 11th International Conference on Electrical Engineering/Electronics, Computer, Telecommunications and Information Technology (ECTI-CON)*. IEEE, 2014, pp. 1–5.

[8] S. Aldhaher, P. C.-K. Luk, and J. F. Whidborne, "Tuning class e inverters applied in inductive links using saturable reactors," *IEEE Transactions on Power Electronics*, vol. 29, no. 6, pp. 2969–2978, 2013.

[9] P. S. Riehl, A. Satyamoorthy, H. Akram, Y.-C. Yen, J.-C. Yang, B. Juan, C.-M. Lee, F.-C. Lin, V. Muratov, W. Plumb *et al.*, "Wireless power systems for mobile devices supporting inductive and resonant operating modes," *IEEE Transactions on Microwave Theory and Techniques*, vol. 63, no. 3, pp. 780–790, 2015.

[10] D. Ahn and P. P. Mercier, "Wireless power transfer with concurrent 200-khz and 6.78-mhz operation in a single-transmitter device," *IEEE Transactions on Power Electronics*, vol. 31, no. 7, pp. 5018–5029, 2015.

[11] M. Liu and M. Chen, "Dual-band wireless power transfer with reactance steering network and reconfigurable receivers," *IEEE Transactions on Power Electronics*, vol. 35, no. 1, pp. 496–507, 2019.